

Effects of helium irradiation dose and temperature on the damage evolution of Ti_3SiC_2 ceramic

Hua-Hai Shen(申华海), Xia Xiang(向霞), Hai-Bin Zhang(张海斌), Xiao-Song Zhou(周晓松), Hong-Xiang Deng(邓洪祥), Xiao-Tao Zu(祖小涛)

Citation: Chin. Phys. B . 2019, 28(7): 076104. **doi:** 10.1088/1674-1056/28/7/076104
Journal homepage: http://cpb.iphy.ac.cn; http://iopscience.iop.org/cpb

What follows is a list of articles you may be interested in

Microstructure and lateral conductivity control of hydrogenated nanocrystalline silicon oxide and its application in a-Si:H/a-SiGe:H tandem solar cells

Tian-Tian Li(李天天), Tie Yang(杨铁), Jia Fang(方家), De-Kun Zhang(张德坤), Jian Sun(孙建), Chang-Chun Wei(魏长春), Sheng-Zhi Xu(许盛之), Guang-Cai Wang(王广才), Cai-Chi Liu(刘彩池), Ying Zhao(赵颖), Xiao-Dan Zhang(张晓丹)
Chin. Phys. B . 2016, 25(4): 046101. **doi:** 10.1088/1674-1056/25/4/046101

FT-Raman spectroscopy study of solvent-in-salt electrolytes

Liumin Suo(索鎏敏), Zheng Fang(方铮), Yong-Sheng Hu(胡勇胜), Liquan Chen(陈立泉)
Chin. Phys. B . 2016, 25(1): 016101. **doi:** 10.1088/1674-1056/25/1/016101

Complementary method to locate atomic coordinates by combined searching method of structure-sensitive indexes based on bond valence method

Song Zhen, Liu Xiao-Lang, He Li-Zhu, Xia Zhi-Guo, Liu Quan-Lin
Chin. Phys. B . 2015, 24(10): 106101. **doi:** 10.1088/1674-1056/24/10/106101

Two-coupled structural modulations in charge-density-wave state of $SrPt_2As_2$ superconductor

Wang Li, Wang Zhen, Shi Hong-Long, Chen Zhen, Chiang Fu-Kuo, Tian Huan-Fang, Yang Huai-Xin, Fang Ai-Fang, Wang Nan-Lin, Li Jian-Qi
Chin. Phys. B . 2014, 23(8): 086103. **doi:** 10.1088/1674-1056/23/8/086103

Single event effect in a ferroelectric-gate field-effect transistor under heavy-ion irradiation

Yan Shao-An, Tang Ming-Hua, Zhao Wen, Guo Hong-Xia, Zhang Wan-Li, Xu Xin-Yu, Wang Xu-Dong, Ding Hao, Chen Jian-Wei, Li Zheng, Zhou Yi-Chun
Chin. Phys. B . 2014, 23(4): 046104. **doi:** 10.1088/1674-1056/23/4/046104

Effects of helium irradiation dose and temperature on the damage evolution of Ti_3SiC_2 ceramic*

Hua-Hai Shen(申华海)[1,†], Xia Xiang(向霞)[2], Hai-Bin Zhang(张海斌)[1], Xiao-Song Zhou(周晓松)[1], Hong-Xiang Deng(邓洪祥)[2,‡], and Xiao-Tao Zu(祖小涛)[2]

[1] *Institute of Nuclear Physics and Chemistry, China Academy of Engineering Physics, Mianyang* 621900, *China*
[2] *School of Physics, University of Electronic Science and Technology of China, Chengdu* 610054, *China*

(Received 14 March 2019; revised manuscript received 8 April 2019; published online 12 June 2019)

The effects of 400 keV helium ion irradiation dose and temperature on the microstructure of the Ti_3SiC_2 ceramic were systematically investigated by grazing incidence x-ray diffraction, scanning electron microscopy, and transmission electron microscopy. The helium irradiation experiments were performed at both room temperature (RT) and 500 °C with a fluence up to 2.0×10^{17} He^+/cm^2 that resulted in a maximum damage of 9.6 displacements per atom. Our results demonstrate that He irradiations produce a large number of nanometer defects in Ti_3SiC_2 lattice and then cause the dissociation of Ti_3SiC_2 to TiC nano-grains with the increasing He fluence. Irradiation induced cell volume swelling of Ti_3SiC_2 at RT is slightly higher than that at 500 °C, suggesting that Ti_3SiC_2 is more suitable for use in a high temperature environment. The temperature dependence of cell parameter evolution and the aggregation of He bubbles in Ti_3SiC_2 are different from those in Ti_3AlC_2. The formation of defects and He bubbles at the projected depth would induce the degradation of mechanical performance.

Keywords: *MAX*, Ti_3SiC_2, helium irradiation, He bubble

PACS: 61.05.–a, 61.05.J–, 61.80.Lj, 81.05.Je **DOI:** 10.1088/1674-1056/28/7/076104

1. Introduction

The layered carbides and nitrides, *MAX* phase ceramics,[1–3] have received much attention since Nowotny first synthesized a large number of carbides.[4] The *MAX* ceramic is generally written as $M_{n+1}AX_n$, where M is an early transition metal, A is an A-group element (mostly IIIA and IVA), and X is either C and/or N. The family of *MAX* ceramics combine many excellent properties of both ceramics and metals, such as good electrical and thermal conductivities, high elastic stiffness, and easy machinability.[1,2,4,5] These properties are due to their unique nano-crystal structure features with a hexagonal structure and $P63/mmc$ symmetry, which can be described as two edge-shared Ti_6C octahedron layers linked by a two-dimensional closed packed A layer.[6–8] The most important character is that the *MAX* phase has outstanding irradiation damage tolerance.[3,6,9–19] Therefore, the *MAX* ceramics are potential candidates for application in future Gen-IV fission reactors and fusion reactors with much higher burn-up, requiring that the material that can survive up to 200 displacements per atom (dpa).[20]

Several *MAX* ceramics have been synthesized or theoretically predicted.[5] Among them, Ti_3SiC_2[3,9,15,18,19,21–23] and Ti_3AlC_2[11,13,14,24,25] are representative materials in the *MAX* phase and have been suggested for the next generation nuclear reactor applications thanks to their advantages of thermal/mechanical properties at high temperature and radiation damage resistance. The irradiation effects on Ti_3SiC_2 and Ti_3AlC_2 subjected to helium[3,12–14,18,19,21,25] and heavy ion[15,16,22,23,26–28] irradiations have been intensively investigated. Spherical He bubbles were formed in Ti_3SiC_2 after He irradiation up to 1.0×10^{18} He^+/cm^2 at room temperature (RT).[14] Tallman *et al.*[6,9] studied the neutron radiation effect in several polycrystalline *MAX* phases, including samples of Ti_3AlC_2, Ti_2AlC, Ti_3SiC_2, and Ti_2AlN. The results showed that the lattice distortion occurred and the dislocation loops formed in the samples of Ti_3SiC_2. Zhang *et al.*[3] found that the high temperature He irradiation and post-annealing offered a path for the recovery of irradiation damages in Ti_3SiC_2. Song *et al.*[19] studied the migration and clustering of He atoms in Ti_3SiC_2 based on the theoretical calculation. Zhang *et al.*[18] revealed the microstructure changes of Ti_3SiC_2 from damage Ti_3SiC_2, damaged TiC precipitation to crystal TiC phase formation due to He irradiation up to 1.0×10^{17} He^+/cm^2. Pang *et al.*[29] illustrated that the structure distortion in Ti_3AlC_2 after combined Fe and He ions irradiation was more serious than that by single Fe-ion irradiation. Flem *et al.*[7] performed the *in-situ* study of 92 MeV Xe ion irradiation damage on $Ti_3(Si,Al)C_2$ materials by using an transmission electron microscope (TEM) to elucidate the deformation mechanism at a very small scale. Different energies of Au and Xe heavy ions irradiations were conducted to the Ti_3SiC_2 material for the purpose of separation of the effects of

*Project supported by the President Foundation of the China Academy of Engineering Physics (Grant No. YZJJLX2018003) and the National Natural Science Foundation of China (Grant No. 21601168).

†Corresponding author. E-mail: huahaishen@caep.cn
‡Corresponding author. E-mail: denghx@uestc.edu.cn

© 2019 Chinese Physical Society and IOP Publishing Ltd

nuclear interactions from those of electronic ones.[17,22]

It was proposed that irradiation would induce substantial crystal structure defects[7,15,28] and cell volume expansion,[26,28] as well as the dissociation of *MAX* to TiC,[6,12] which contributed to the volumetric swelling of the *MAX* phases.[30] Usually, the amorphization of nuclear materials would lead to degraded corrosion resistance and the materials become brittle,[31,32] so the transformation of *MAX* phases from crystalline to amorphous under irradiation was considered to inevitably contribute to the degradation of the mechanical property. Up to now, the previous studies suggested that the *MAX* phases have not been completely amorphized even the irradiation dose up to 116.9 dpa.[23] The remarkable irradiation resistance of *MAX* ceramics was suggested to be ascribed to the *A* layer atoms offering the space to accommodate point defects.[9,10] Besides, Shen *et al.*[23] proposed that the Xe^+ irradiation induced TiC nanograins enhanced the irradiation tolerance of Ti_3SiC_2 ceramic because the formation of nanograins provided a higher density of boundaries.[14] Helium irradiation caused the lattice expansion of Ti_3SiC_2 at a low irradiation dose and induced the phase transformation from Ti_3SiC_2 to crystal TiC phase.[18] Wang *et al.*[8] directly observed the mixing of Ti and Al atoms under Au ion bombardment at atomistic-scale resolution, as well as the formation of fcc-$(Ti_3Al)C_2$ phases.

Although the effects of ion irradiation on Ti_3SiC_2 have been reported before by Nappé *et al.*,[27] Whittle *et al.*,[16] Zhang *et al.*,[15] Shen *et al.*,[23] and Zhang *et al.*[3,18] A systematic TEM investigation of the He irradiation damage with respect to fluence and temperature is still necessary to understand the evolution and mechanism of He bubbles in Ti_3SiC_2 lattice. In this work, the Ti_3SiC_2 bulk samples are irradiated with 400 keV He^+ ions at both RT and 500 ℃. The irradiation induced damages are characterization by grazing incidence x-ray diffraction (GIXRD) and TEM. The irradiation induced defects are accurately obtained by comparing the microstructure in the irradiated area with that in the un-irradiated area from the same Ti_3SiC_2 grain. The correlations between the irradiation damage and dose and temperature are analyzed and discussed.

2. Experimental methods

2.1. Sample preparation

The Ti_3SiC_2 bulk samples used in this study were synthesized by a hot pressing method.[23,25] The Ti (99%, 200 mesh), Si (99%, 300 mesh), and graphite (99%, 200 mesh) powders with a molar ratio of 3 : 1.2 : 2 were weighted and used as the starting materials for synthesizing Ti_3SiC_2 ceramic. The Ti, Si, and C powders were dry mixed in a resin jar, followed by ball milling for 12 h, and then sieved. The mixture powders were put into a graphite die and uniaxially pressed at 5 MPa, and then heated to a desired temperature of 1550 ℃ and hold for 1 h under an Ar atmosphere. The as-obtained bulk sample was finally cooled down to RT and pressed for 5 min. The bulk specimens used for irradiation and characterization have a size of 5 mm (L) ×5 mm (W) ×3 mm (T), and were prepared by cutting into pieces using a diamond saw and mechanically polishing to remove the surface contamination.

2.2. Helium irradiation

The He irradiation experiments were performed at Michigan Ion Beam Laboratory in University of Michigan. The ion implantation energy was set at 400 keV with the sample normal direction, which would result in a projected range of 1330 nm that was calculated by SRIM code.[33,34] The SRIM code was also used to simulate the He irradiation induced damage and He concentrations in the Ti_3SiC_2 matrix and the used displacement energies were 25 eV, 25 eV, and 28 eV for Ti, Si, and C,[12,35] respectively. The helium fluence was in a range from 0.5×10^{17} He^+/cm^2 to 2.0×10^{17} He^+/cm^2, and the helium flux was set at 0.78×10^{14} $He^+/(cm^2 \cdot s)$ to avoid the severe irradiation heating.[8] With the aim to understand the effect of temperature on the irradiation damage in the Ti_3SiC_2 ceramic, the temperature was kept at both RT and 500 ℃ during the irradiation. The detailed irradiation parameters can be found in Table 1. The irradiation induced damage and He concentration as a function of depth are shown in Fig. 1. It is clear that the He irradiations with the fluences of 0.5×10^{17} He^+/cm^2, 1.0×10^{17} He^+/cm^2, and 2.0×10^{17} He^+/cm^2 cause the damages of 2.4 dpa, 4.8 dpa, and 9.6 dpa at the depth of 1330 nm, respectively. The He concentration at the projected depth increases from 3.2 at.% for the 0.5×10^{17} He^+/cm^2 fluence to 11.5 at.% for the 2.0×10^{17} He^+/cm^2 one. The specimens are designated based on the irradiation conditions and listed in Table 1 as LT2.4, LT4.8, LT9.6 for RT irradiations and HT2.4, HT4.8, HT9.6 for 500 ℃ irradiations.

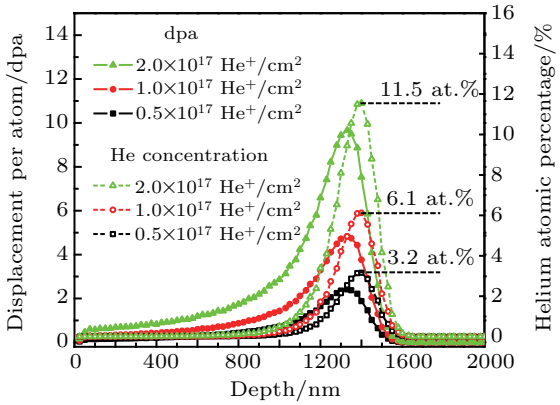


Fig. 1. SRIM results of 400 keV helium irradiation on Ti_3SiC_2 to fluence of 0.5×10^{17} He^+/cm^2, 1.0×10^{17} He^+/cm^2, and 2.0×10^{17} He^+/cm^2, which induced a maximal damage of 2.4 dpa, 4.8 dpa, and 9.6 dpa at the project depth of 1330 nm, respectively.

Table 1. The detailed conditions for helium irradiation and the induced damages at the projected depth of 1330 nm in the as-implanted sample based on the SRIM calculation.

Temperature/°C	Implantation energy/keV	Helium fluence /10^{17} $He^+ \cdot cm^2$	Irradiation damage/dpa	Helium concentration at projected depth/at.%	Sample designation
RT	400	0.5	2.4	3.2	LT2.4
		1.0	4.8	6.1	LT4.8
		2.0	9.6	11.5	LT9.6
500		0.5	2.4	3.2	HT2.4
		1.0	4.8	6.1	HT4.8
		2.0	9.6	11.5	HT9.6

2.3. Microstructure characterizations

After irradiation, the cross-sectional TEM specimens with thickness of around 100 nm were prepared by a focused ion beam (FIB) lift-out technique in a Helios 650 Nanolab workstation.[36] The detailed FIB procedures for the TEM sample preparation could be found elsewhere.[36] Due to the extreme thin irradiation surface layer, the structures of the irradiated samples were examined by GIXRD using an X'pert PRO MPD with a Cu $K\alpha$ radiation working at 40 kV and 40 mA. The typical parameters for collecting the GIXRD patterns were 30°–45° in 2θ range, 0.02° in step size, and 3 s in step time. The grazing angle was set to 2.3°, which corresponds to an x-ray penetration depth of 1350 nm calculated by Mass-Absorption-Calculator in X'Pert Highscore software using the density of Ti_3SiC_2 (4.52 g/cm^3).[1,2] The sample surface morphologies were observed using a Helios 650 Nanolab SEM, which was equipped with an energy dispersive spectroscopy (EDS) utilized to acquire the element distribution of Ti, Si, and C. The microstructures and crystal structures of the irradiated samples were examined by bright-field image (BF), annular dark-field image (ADF), and selected area electron diffraction (SAED) of a JEOL 2010 F TEM operating at 200 kV with both TEM and STEM modes. The high resolution TEM (HRTEM) image was captured to obtain the shape and distribution of the He bubbles.

3. Results

3.1. Microstructure of Ti_3SiC_2 virgin sample

An SEM image of surface morphology of pristine Ti_3SiC_2 sample is shown in Fig. 2(a) and the corresponding EDS mapping images of Ti and Si elements from the area in Fig. 2(a) are shown in Figs. 2(b) and 2(c). Figure 2(d) shows the XRD pattern of the pristine Ti_3SiC_2 sample, showing that the pristine sample consists of the majority phase of Ti_3SiC_2 and some impurity phases of SiC and TiC. The Ti_3SiC_2 has a hexagonal structure with $P63/mmc$ symmetry and the lattice parameters (LP) are $a = 0.3072$ nm and $c = 1.7677$ nm. The pristine Ti_3SiC_2 shows a layered and lath-shaped feature with grain size (in length) of over 5 μm, as shown in Fig. 2(a). According to EDS mapping results, the SiC and TiC impurity phases cover areas of ∼ 8.8% and ∼ 6.8%, respectively.

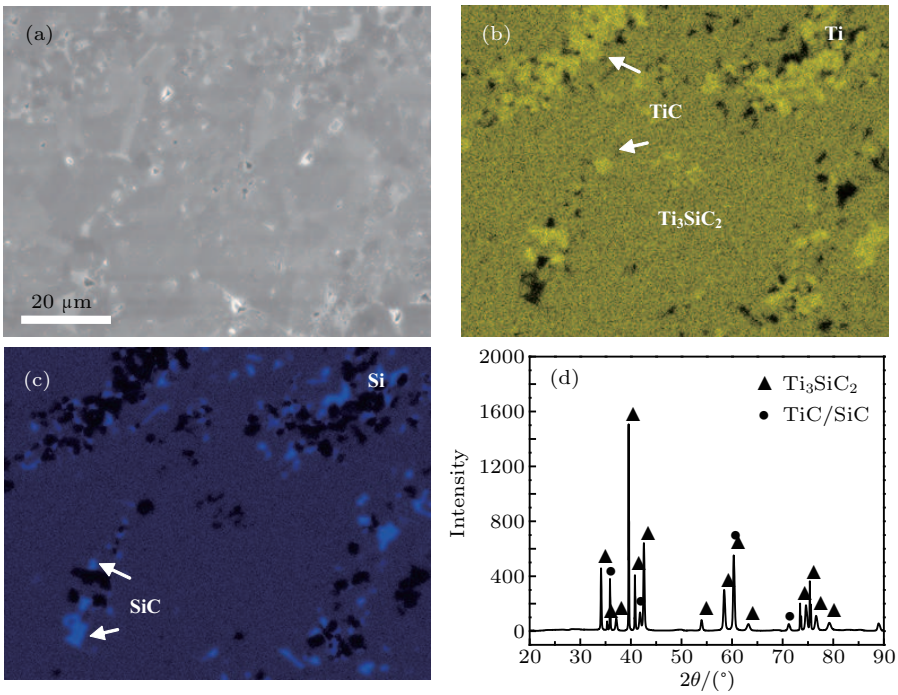


Fig. 2. (a) SEM image of Ti_3SiC_2 before irradiation. EDS mapping of (b) Ti and (c) Si elements from the area shown in (a). (d) XRD pattern acquired from Ti_3SiC_2 before irradiation.

The SAED pattern obtained in TEM analysis confirms the crystal structure of the Ti_3SiC_2 sample. A TEM lamellar of the pristine sample across the interface between Ti_3SiC_2 grains and impurity phases was prepared by an FIB lift-out method. Figures 3(a) and 3(b) show the STEM-ADF image and EDS mapping of Si element of the pristine Ti_3SiC_2 sample. The SAED patterns taken from the Ti_3SiC_2 grain and the Si-enrich area are shown in Figs. 3(c) and 3(d), which are indexed as Ti_3SiC_2 and SiC phases with the zone axes of $[10\bar{1}0]$ and [110].

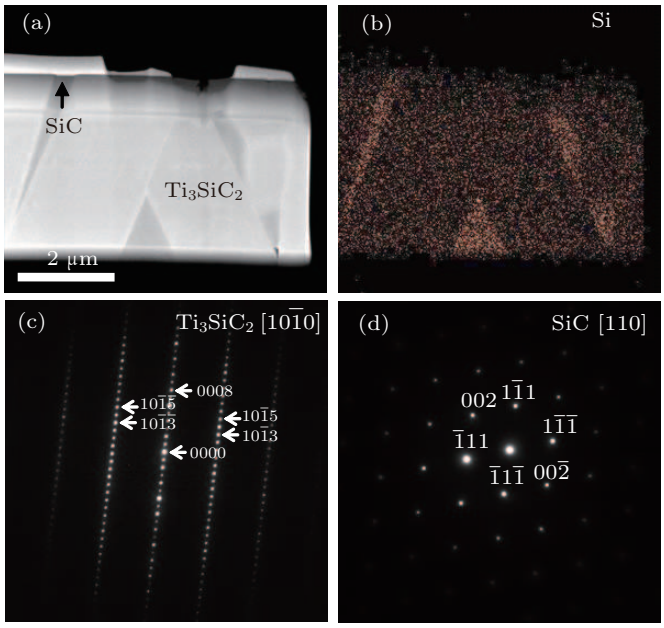


Fig. 3. (a) STEM-ADF image of a Ti_3SiC_2 TEM specimen prepared by FIB method cutting across grain boundaries of Ti_3SiC_2 and impurity phases. (b) EDS mapping of Si element of the area shown in (a). (c) and (d) SAED patterns taken from the Ti_3SiC_2 and impurity phase grains along the viewing directions of $[10\bar{1}0]$ and [110], respectively.

3.2. He irradiation induced microstructure changes

Figure 4 shows a series of SEM images for the Ti_3SiC_2 samples irradiated at RT (Figs. 4(a)–4(c)) and 500 ℃ (Figs. 4(d)–4(f)). No significant morphology change has been found on the surface for all irradiation conditions. In comparison, significant grain boundary cracking was found by Huang *et al.*[35] and Clark *et al.*[26] in Ti_3AlC_2. Helium irradiation induced the anisotropic swelling of the Ti_3AlC_2 structure, which provided the driven energy for the formation of cracks.[30] Surface exfoliation was found on Ti_3AlC_2 after He irradiation to 1.0×10^{17} He^+/cm^2 at RT.[25] This result implied the different irradiation effect and He bubble evolution mechanism in Ti_3SiC_2 and Ti_3AlC_2. Therefore, it is supposed that Ti_3SiC_2 exhibits better irradiation resistance than Ti_3AlC_2.

Figures 5 and 6 show the BF images and SAED patterns of Ti_3SiC_2 samples after He ion irradiation at RT and 500 ℃, respectively. A damaged surface layer is clearly shown in the BF images and the thickness of the damaged layer is consistent with the calculated results by SRIM code. For each BF image of the sample irradiated at different condition, three zones coexist; i.e., FIB-Pt zone, irradiation damaged zone, and non-irradiated zone. In order to analyze the irradiation induced damage, two SAED patterns were taken from the irradiated zone and non-irradiated bulk areas in the same Ti_3SiC_2 grain.

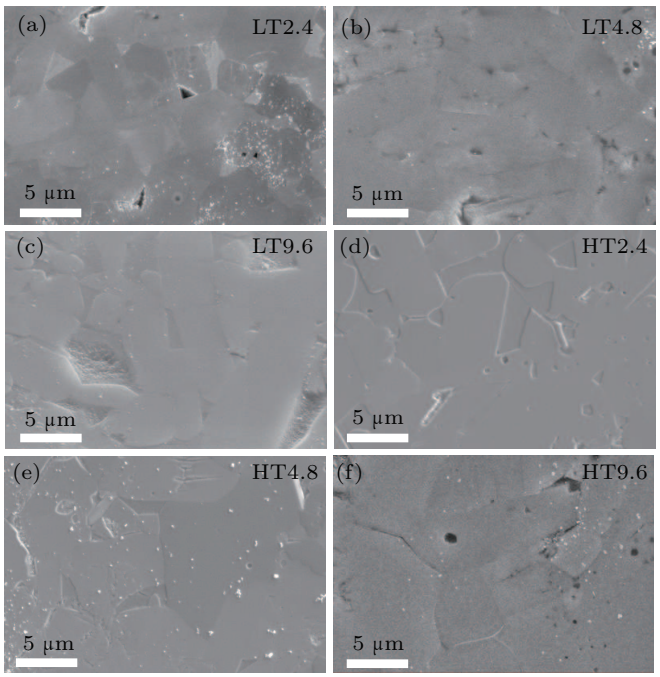


Fig. 4. SEM images of Ti_3SiC_2 specimens after He irradiation up to 2.0×10^{17} He^+/cm^2 at (a)–(c) RT or (d)–(f) 500 ℃.

At RT, for the LT2.4 specimen, the SAED patterns from the irradiated and non-irradiated areas in Fig. 5(a) are shown in Figs. 5(b) and 5(c). Both patterns can be indexed as Ti_3SiC_2 with the zone axis of $[21\bar{3}0]$. There is no remarkable difference between these patterns, indicating that the Ti_3SiC_2 lattice refrains from severe damage of 2.4 dpa He^+ irradiation. After being irradiated to 4.8 dpa, it is clear in Fig. 5(f) that some diffraction spots labeled become much brighter, while others become slightly weakened. It is worth mentioning that the labeled spots can also be indexed as TiC with fcc structure along [110] direction, implying the dissociation of Ti_3SiC_2 to TiC. The formation of TiC due to neutron and He ion irradiation has been reported by Tallman *et al.*[6] and Song *et al.*[6,12] With dose increasing up to 9.6 dpa, all of the spots viewing from the $[10\bar{1}0]$ direction become significantly diffused, which is likely to be due to the production of much more structural defects. The completely amorphous ring was not observed for the highest irradiation dose, indicating the excellent irradiation resistance of Ti_3SiC_2.

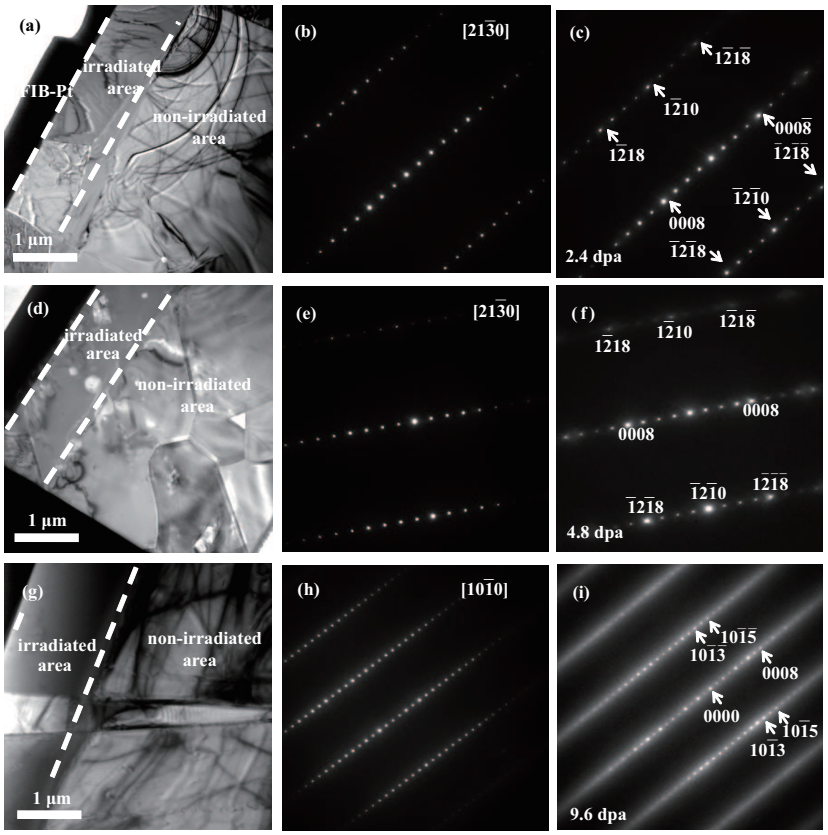


Fig. 5. BF images of specimens (a) LT2.4, (d) LT4.8, and (g) LT9.6. Helium irradiation induced an irradiated layer with a thickness around 1330 nm, which was followed by the non-irradiated bulk. The corresponding SAED patterns taken from the non-irradiated area and irradiated area are respectively shown in panels (b), (e), (h) and (c), (f), (i). The SAED patterns in panels (b), (e), and (h) are indexed with the zone axes of [21$\bar{3}$0], [21$\bar{3}$0], and [10$\bar{1}$0], respectively.

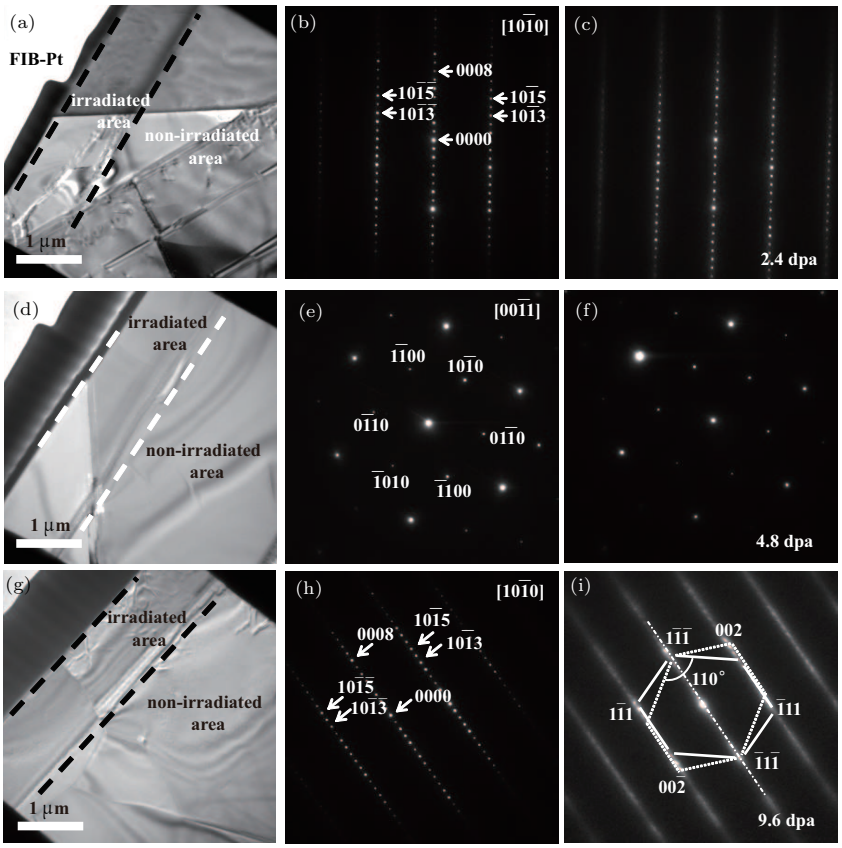


Fig. 6. BF images of specimens (a) HT2.4, (d) HT4.8, and (g) HT9.6. The corresponding SAED patterns taken from the non-irradiated area and irradiated area are respectively shown in panels (b), (e), (h) and (c), (f), (i). The SAED patterns in panels (b), (e), and (h) are indexed with the zone axes of [10$\bar{1}$0], [0001], and [10$\bar{1}$0], respectively. (i) With increasing irradiation dose, the diffraction spots in SAED pattern become dispersed at 9.6 dpa.

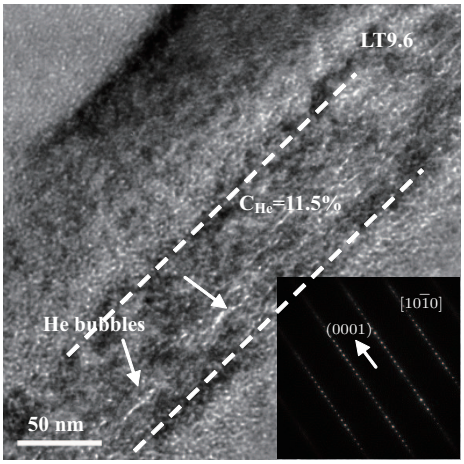


Fig. 7. BF image of LT9.6 specimen in which a lot of He bubbles formed at the projected depth. The inset shows the SAED pattern taken from this area.

Figure 7 shows a HRTEM image acquired from the projected layer of LT9.6, in which the inset presents the SAED pattern taken from the same area. A great many of individual He bubbles were formed in this area due to the aggregation of He atoms. It can also be found that some He bubbles start to merge into a string lying on a preferential plane of Ti_3SiC_2 (0001).[37] It is well-known that the Si layer, having larger lattice space, represents nano-scale interfaces that function as natural sinks for defects.[9,30] Zhang *et al.*[21] observed that helium atoms prefer to accumulate within the layers where Si atoms have been dislodged creating 2-dimensional channels. Song *et al.*[19] demonstrated by theoretical calculation that the largest He clusters with no more than 7 He atoms were formed in the Si layer.

At 500 ℃, for the HT2.4 specimen, the SAED patterns taken from the non-irradiated and irradiated areas are shown in Figs. 6(b) and 6(c), respectively. The SAED patterns are indexed as [10$\bar{1}$0] zone axis of Ti_3SiC_2. No apparent change is found by comparing these SAED patterns, which is in accord with that for the LT2.4 specimen. After irradiated to 4.8 dpa, there is no discrepancy between the SAED patterns before and after irradiation. This might be due to that the high temperature provides more energy for the annihilation of point defects. Moreover, it is well-known that irradiated induced defects in Ti_3SiC_2 are preferred to accumulate in the Si layer,[9,21] thus it is not clear to see the defects from the viewing direction close to *c*-axis. Once the dose increased to 9.6 dpa, most of the diffraction spots become weakened or almost disappear, while others are no longer circular and start to evolve to polycrystalline rings. These transformations should be attributed to the structure distortion or the disappearance of Ti_3SiC_2 nanolamellar structure.[38] The diffraction spots labeled in Fig. 6(h) for the Ti_3SiC_2 phase can also be indexed as the twin crystal of TiC phase with angle of 110° along [11$\bar{2}$0] viewing direction. The labeled spots of TiC overlap with those polycrystalline rings, which indicates that He irradiation causes the Ti_3SiC_2 grain broken and leads to the formation of TiC nanograins.[15]

Figure 8 shows the GIXRD patterns collected from the virgin sample and the specimens irradiated at RT and 500℃ to different doses. All of patterns have been indexed as Ti_3SiC_2 phase, where the three major peaks are labeled as (10$\bar{1}$1), (10$\bar{1}$4), and (10$\bar{1}$5). It should be pointed out that subtle changes were found on (10$\bar{1}$4) and (10$\bar{1}$5) peaks. These two peaks shift towards to lower 2θ angles, suggesting that a crystal distortion occurred after irradiation. At RT, the position of the (10$\bar{1}$5) peak continuously drops with the increasing He fluence. In comparison, the crystal structure of Ti_3SiC_2 would not be seriously modified with the He irradiation fluence at 500 ℃. The structure parameters of Ti_3SiC_2, *a*-LP, *c*-LP, and cell volume, derived from the GIXRD patterns are tabulated in Table 2.

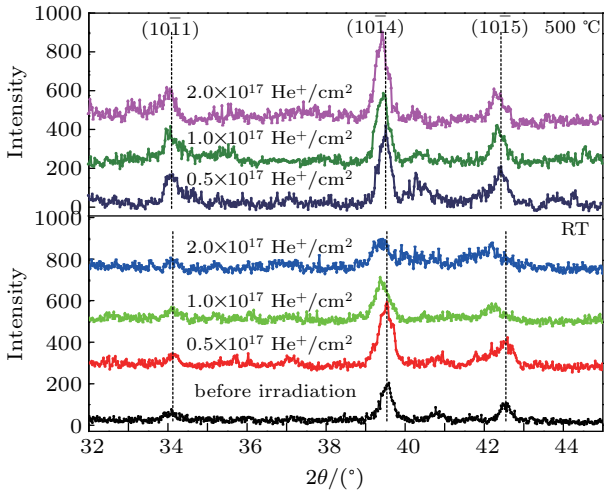


Fig. 8. GIXRD patterns of Ti_3SiC_2 specimens after He irradiation at (b) RT and (a) 500 ℃ with fluence increasing from 0.5×10^{17} He$^+$/cm^2 to 2.0×10^{17} He$^+$/cm^2.

At RT, a slight reduction of *a*-LP and an obvious expansion of *c*-LP, leading to the volume expansion of 0.74%, are observed after irradiated to 2.4 dpa, as shown in Fig. 9. With the dose increasing from 2.4 dpa to 9.6 dpa, the expansion of *c*-LP increases remarkably from 0.74% to 2.53%, leading a volume swelling from 0.21% to 1.93%. However, *a*-LP seems to be independent of the He fluence. These results should be attributed to the formation of defects[6,28] in the lattice and the He bubbles in the Si layer,[13,14] which is consistent with the HRTEM observation that He bubbles lying on the (0001) plane. The FWHMs of the (10$\bar{1}$4) and (10$\bar{1}$5) peaks after Ti_3SiC_2 irradiated under different conditions are listed in the last two rows of Table 2. Both of the (10$\bar{1}$4) and (10$\bar{1}$5) peaks broaden with the increasing He fluence, especially for the (10$\bar{1}$5) peak where its FWHM increases from 0.29° to 0.98° after irradiated to 9.6 dpa. This peak broadening exhibits the production of much more defects in the corresponding crystal plane, which alternately induces the loss of crystallinity of Ti_3SiC_2.

Table 2. The Ti_3SiC_2 crystal structure parameters, *a*-LP, *c*-LP, and cell volume, calculated from the GIXRD patterns (Fig. 8) of the specimens before and after He irradiation. The full widths at half maximal (FWHMs) of $(10\bar{1}4)$ and $(10\bar{1}5)$ peaks after Ti_3SiC_2 specimens irradiated under different conditions are listed in the last two rows.

Structure parameters	Virgin	LT2.4	LT4.8	LT9.6	HT2.4	HT4.8	HT9.6
a-LP/nm	0.3072	0.3064	0.3065	0.3063	0.3063	0.3067	0.3076
a-LP shrinkage/%	/	–0.26%	–0.23%	–0.29%	–0.29%	–0.16%	0.13%
c-LP/nm	1.7677	1.7807	1.7984	1.8124	1.7843	1.7849	1.7752
c-LP expansion/%	/	0.74%	1.74%	2.53%	0.94%	0.97%	0.42%
Cell volume/Å^3	144.47	144.78	146.31	147.26	144.97	145.40	145.46
Cell volume expansion/%	/	0.21%	1.27%	1.93%	0.35%	0.64%	0.69%
$(10\bar{1}4)$	0.31°	0.42°	0.44°	0.45°	0.35°	0.38°	0.36°
$(10\bar{1}5)$	0.29°	0.50°	0.56°	0.98°	0.41°	0.38°	0.40°

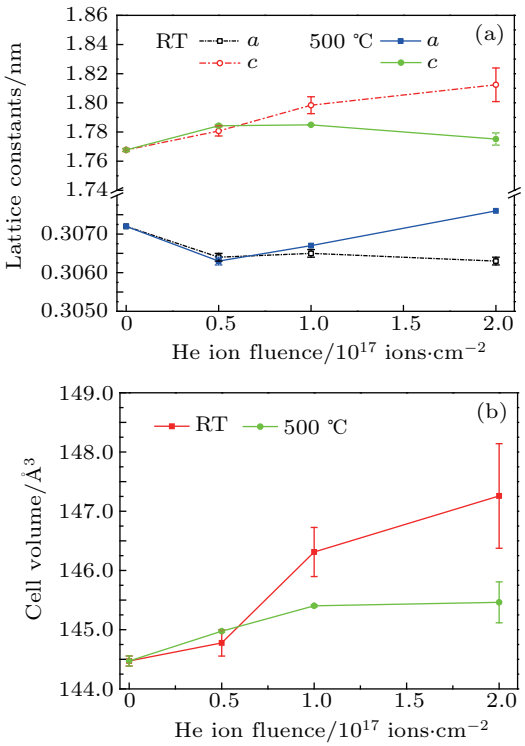


Fig. 9.(a) The *a*-LP, *c*-LP and (b) cell volume of Ti_3SiC_2 change as a function of irradiation temperature and fluence.

At 500 ℃, the reduction of *a*-LP and the expansion of *c*-LP are 0.29% and 0.94%, respectively. However, with the dose increasing from 2.4 dpa to 9.6 dpa, *a*-LP starts to expand to 0.13%, while the expansion of *c*-LP drops from 0.94% to 0.42%, indicating that the Ti_3SiC_2 cell starts to recover with the higher He fluence. This phenomenon is contrary to the result from the RT irradiation. The FWHMs of the $(10\bar{1}4)$ and $(10\bar{1}5)$ peaks both show a slight broadening after 2.4 dpa irradiation, and then have a tiny change with the post-irradiation. It can be concluded that Ti_3SiC_2 has better irradiation resistance at high temperature compared to that at RT, which might be due to the higher annihilation of point defects at high temperature.

4. Discussion

The SAED results demonstrate that the dissociation of Ti_3SiC_2 to TiC phase occurred after He irradiation, which has been reported by Tallman *et al.*[9] Shen *et al.*[23,25] demonstrated that the Xe and He ion irradiation would induced the formation of TiC nanograins in Ti_3SiC_2 and Ti_3AlC_2 ceramics. The precipitation of TiC nanograins would be beneficial for improving the irradiation resistance of *MAX* ceramics. The dissociation of Ti_3SiC_2 has been well explained by theoretical calculations that the bonding between Ti and Si is relatively weaker than Ti–C bonds, which can induce the removal of the Si layer leaving the TiC unperturbed.[14] Zhang *et al.*[3] found that He bubble aggregation in Si layer at high temperature provided a path for Si loss and the formation of TiC nanograins. The mechanism of the formation of fcc-TiC phase has been clearly understood in atomistic scale by Wang *et al.*[8] Under Au ion irradiation, the Al atoms would left their original sites and enter the TiC lattice to randomly replace the Ti atoms and to form the metastable γ-$(Ti_3Al)C_2$ and the fcc-$(Ti_3Al)C_2$ phases.[8] Therefore, the fcc phase product formed during the dissociation of Ti_3SiC_2 phase should be ascribed to the formation of fcc-$(Ti_3Si)C_2$ while the Si atoms enter the TiC lattice and occupy the Ti sites.

At both RT and 500 ℃, the SAED and GIXRD results revealed the volume swelling after He irradiation, which could be easily understood that the He bubbles aggregating at the Si layer induce the *c*-LP expansion and volume expansion.[13,14] In comparison, the volume expansion of Ti_3SiC_2 increases remarkably with the increasing He fluence at RT, while it shows a slight increase at 500 ℃. This may imply the different mechanisms of He atoms diffusion in the Ti_3SiC_2 lattice. It is well-known that the Si layer, having larger lattice space, represents nano-scale interfaces that function as natural sinks for He atoms and defects.[9,30] The presence of Si layer is responsible for the outstanding irradiation resistance of Ti_3SiC_2 phase. Therefore, it is easily understood that the He bubbles grow along the *c*-plane with the post-irradiation and induce the *c*-LP expansion at RT and 500 ℃.

The mechanism of He bubble aggregation is proposed to interpret the different changing tendencies of Ti_3SiC_2 cell parameters irradiated at RT and 500 ℃. Figure 10 shows the schematic atomic arrangement of Ti_3SiC_2 crystal structure viewing from $[11\bar{2}0]$ direction. As reported by Nowotny,[4]

Ti_3SiC_2 material has a structure with 2-dimension close-packed Si intercalating into the TiC lattice.[21] TiC twin crystals are separated by the Si layer with an angle of 110°.[39] It is evident that the interaction between Ti and C atoms is quite strong,[1,10,21,24,38] it is hard for the He atoms incorporating into the TiC lattice. However, it was proposed that the irradiation would produce a lot of point defects in the TiC lattice, which can further induce the contraction of TiC and Ti_3SiC_2 lattices. At RT, the density of radiation defect increased with the increasing He fluence, which would cause the continuously shrinkage of *a*-LP in Ti_3SiC_2.

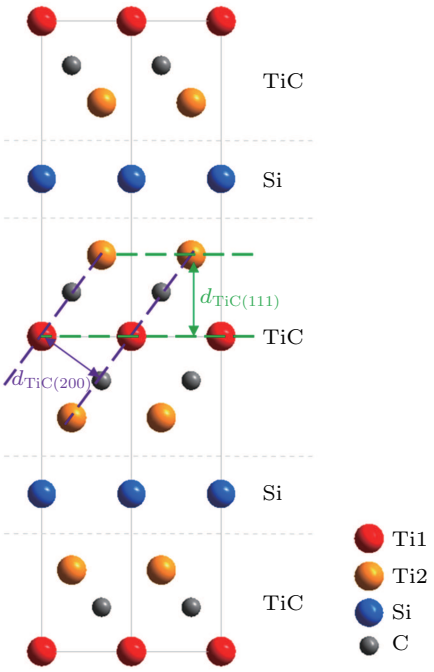


Fig. 10. The atomic arrangement of Ti_3SiC_2 crystal structure viewing from $[11\bar{2}0]$ direction.

In contrast, the He bubbles exhibited different diffusion and aggregation mechanism at 500 ℃. Once the defects formed in the TiC lattice, they would play an important role as natural sinks for He atoms. Song *et al.*[21] found that the He atoms could be trapped by vacancies in the C layer based on the first-principles calculation. For fcc-TiC, the {111} plane is the habit plane with lower formation energy of defect. The implanted He atoms tend to incorporated into the {111} planes.[40] As shown in Fig. 10, the (111) and (200) planes of TiC phase are parallel to the $(10\bar{1}3)$ and $(10\bar{1}5)$ of Ti_3SiC_2 phase. The accumulation of He bubbles on the {111} planes induces the expansion along *c* direction of Ti_3SiC_2. It was reported that the He bubble induced expansion of {111} planes would allow the {200} planes to expand more uniformly for fcc-ErT_2.[41] From the arrangement of Ti_3SiC_2, the $(20\bar{2}0)$ plane lies at 55° to the *a* direction of Ti_3SiC_2. The expansion of two (200) planes of twin TiC crystals would arise a larger expansion in the *a* direction of Ti_3SiC_2. As a result, we believe that this expansion contributes to the *a*-LP expansion of Ti_3SiC_2 with the increasing He ion fluence above 0.5×10^{17} He^+/cm^2, which is in accord with the GIXRD results. Zhang *et al.*[21] found that the He atoms would diffuse out of the He bubble formed on Si layer, enabling the diffusion of mobile Si back to their original sites at high temperature. This fact indicates that the He atoms are not energetically stable at the Si layer, and prefer to be trapped by the defects in the TiC lattice at high temperature irradiation. Moreover, the high temperature annealing was suggested to play a positive role in the recovery of He irradiation damage in Ti_3SiC_2,[3] which manifested the decrease of *c*-LP with increasing He fluence above 0.5×10^{17} He^+/cm^2 very well in this study.

In comparison to Ti_3AlC_2,[36] Ti_3SiC_2 exhibited a better irradiation resistance that was conforming to the results of Tallman *et al.*[11] and Shen *et al.*[23] The most important reasons should be ascribed to the absence of surface exfoliation and smaller volume expansion in Ti_3SiC_2 after He irradiation. It seems that the temperature dependence of cell parameters in Ti_3SiC_2 under He irradiation was different from that in Ti_3AlC_2,[23] which has been well explained by the different migration and aggregation of He atoms in Ti_3SiC_2 and Ti_3AlC_2. The detailed investigation of He atom diffusion and defect evolution at an atomistic scale is still preferred for understanding the different irradiation effects in Ti_3SiC_2 and Ti_3AlC_2. Meanwhile, the Ti_3SiC_2 ceramic should be more suitable for using at high temperature environment due to the high annihilation of the irradiation defects.[9,18,19,21]

5. Conclusions

The He irradiation damage on Ti_3SiC_2 with different He fluence and irradiation temperature was systematically investigated by GIXRD, SEM, EDS, and SAED techniques. Helium irradiation of 2.0×10^{17} He^+/cm^2 fluence causes a maximal damage of 9.6 dpa at the projected depth. At both RT and 500 ℃, the results show that He irradiations produce a large number of defects in the Ti_3SiC_2 lattice, which evolve to the dissociation of Ti_3SiC_2 to TiC with the increasing He fluence. At RT, the cell volume swelling of Ti_3SiC_2 increases continuously with the He fluence, indicating the accumulation of He bubbles on the Si layers. In comparison, the volume of Ti_3SiC_2 shows a slight swelling during irradiation at 500 ℃, while the *a*-LP starts to expand at higher He fluence. This suggests that the He bubbles prefer to migrate into the TiC lattice rather than the Si layer at higher temperature. It is evident that the changing tendency of the cell parameter and the He bubble aggregation in Ti_3SiC_2 is significantly different from that in Ti_3AlC_2. It is proposed that Ti_3SiC_2 is more suitable for use in a high temperature environment and exhibits better irradiation resistance than Ti_3AlC_2.

References

[1] Barsoum M W 2000 *Prog. Solid St. Chem.* **28** 201
[2] Barsoum M W and El-Raghy T 1996 *J. Am. Ceram. Soc.* **79** 1953
[3] Zhang H, Su R, Shi L, O'Connor D J, King B V and Kisi E H 2018 *J. Eur. Ceram. Soc.* **38** 1253
[4] Nowotny V H 1971 *Prog. Solid St. Chem.* **5** 27
[5] Ching W Y, Mo Y, Aryal S and Rulis P 2013 *J. Am. Ceram. Soc.* **96** 2292
[6] Tallman D J, Hoffman E N, Caspi E a N, Garcia-Diaz B L, Kohse G, Sindelar R L and Barsoum M W 2015 *Acta Mater.* **85** 132
[7] Le Flem M, Liu X, Doriot S, Cozzika T and Monnet I 2010 *Int. J. Appl. Ceram. Technol.* **7** 766
[8] Wang C, Yang T, Tracy C L, Lu C, Zhang H, Hu Y J, Wang L, Qi L, Gu L, Huang Q, Zhang J, Wang J, Xue J, Ewing R C and Wang Y 2019 *Nat. Commun.* **10** 622
[9] Tallman D J, He L, Garcia-Diaz B L, Hoffman E N, Kohse G, Sindelar R L and Barsoum M W 2016 *J. Nucl. Mater.* **468** 194
[10] Zhao S, Xue J, Wang Y and Huang Q 2014 *J. Appl. Phys.* **115** 023503
[11] Yang T, Wang C, Taylor C A, Huang X, Huang Q, Li F, Shen L, Zhou X, Xue J, Yan S and Wang Y 2014 *Acta Mater.* **65** 351
[12] Song P, Sun J, Wang Z, Cui M, Shen T, Li Y, Pang L, Zhu Y, Huang Q and Lü J 2014 *Nucl. Instrum. Methods Phys. Res. Sect. B* **326** 332
[13] Patel M K, Tallman D J, Valdez J A, Aguiar J, Anderoglu O, Tang M, Griggs J, Fu E, Wang Y and Barsoum M W 2014 *Scr. Mater.* **77** 1
[14] Wang C, Yang T, Kong S, Xiao J, Xue J, Wang Q, Hu C, Huang Q and Wang Y 2013 *J. Nucl. Mater.* **440** 606
[15] Zhang L, Qi Q, Shi L Q, O'Connor D J, King B V, Kisi E H and Venkatachalam D K 2012 *Appl. Surf. Sci.* **258** 6281
[16] Whittle K R, Blackford M G, Aughterson R D, Moricca S, Lumpkin G R, Riley D P and Zaluzec N J 2010 *Acta Mater.* **58** 4362
[17] Nappé J C, Grosseau P, Audubert F, Guilhot B, Beauvy M, Benabdesselam M and Monnet I 2009 *J. Nucl. Mater.* **385** 304
[18] Zhang H, Su R, Shi L, O'Connor D J and Wen H 2018 *Appl. Surf. Sci.* **434** 1210
[19] Song Q, Zhang P, Zhuang J and Ning X J 2017 *Comp. Mater. Sci.* **137** 327
[20] Zinkle S J and Snead L L 2014 *Annu. Rev. Mater. Res.* **44** 241
[21] Zhang H F, Yao B D, Shi L Q, O'Connor D J, Huang J, Zhang J Y, Ding W and Wang Y X 2015 *Acta Mater.* **97** 50
[22] Nappé J C, Monnet I, Audubert F, Grosseau P, Beauvy M and Benabdesselam M 2012 *Nucl. Instrum. Methods Phys. Res. Sect. B* **270** 36
[23] Shen H H, Li F Z, Zhang H B, Peng S M, Zu X T and Sun K 2017 *J. Eur. Ceram. Soc.* **37** 855
[24] Xiao J, Wang C, Yang T, Kong S, Xue J and Wang Y 2013 *Nucl. Instrum. Methods Phys. Res. Sect. B* **304** 27
[25] Shen H H, Ao L, Li F Z, Peng S M, Zhang H B, Sun K and Zu X T 2017 *J. Nucl. Mater.* **485** 262
[26] Clark D W, Zinkle S J, Patel M K and Parish C M 2016 *Acta Mater.* **105** 130
[27] Nappé J C, Maurice C, Grosseau P, Audubert F, Thomé L, Guilhot B, Beauvy M and Benabdesselam M 2011 *J. Eur. Ceram. Soc.* **31** 1503
[28] Liu X, Le Flem M, Béchade J L, Onimus F, Cozzika T and Monnet I 2010 *Nucl. Instrum. Methods Phys. Res. Sect. B* **268** 506
[29] Pang L L, Li B S, Shen T L, Gao X, Fang X S, Gao N, Yao C F, Wei K F, Cui M H, Sun J R, Chang H L, He W H, Huang Q and Wang Z G 2018 *Chin. Phys. Lett.* **35** 026102
[30] Ang C, Silva C, Shih C, Koyanagi T, Katoh Y and Zinkle S J 2016 *Scr. Mater.* **114** 74
[31] Lee Y S, Huang K Y, Huang C Y, Kai J J and Hsieh W F 1993 *J. Nucl. Mater.* **205** 476
[32] Lefebvre F and Lemaignan C 1989 *J. Nucl. Mater.* **165** 122
[33] Ziegler J F, Ziegler M D and Biersack J P 2010 *Nucl. Instrum. Methods Phys. Res. Sect. B* **268** 1818
[34] Shen H H, Peng S M, Zhou X S, Sun K, Wang L M and Zu X T 2014 *Chin. Phys. B* **23** 36102
[35] Huang Q, Liu R, Lei G, Huang H, Li J, He S, Li D, Yan L, Zhou J and Huang Q 2015 *J. Nucl. Mater.* **465** 640
[36] Shen H H, Peng S M, Xiang X, Naab F N, Sun K and Zu X T 2014 *J. Nucl. Mater.* **452** 335
[37] Wang H F, Peng S M, Ding W, Shen H H, Wang W D, Zhou X S and Long X G 2018 *Chin. Phys. B* **27** 96103
[38] Middleburgh S C, Lumpkin G R and Riley D 2013 *J. Am. Ceram. Soc.* **96** 3196
[39] Zhou Y and Sun Z 2000 *Mater. Res. Innovat.* **3** 286
[40] Dickerson C, Yang Y and Allen T R 2012 *J. Nucl. Mater.* **424** 62
[41] Rodriguez M A, Browning J F, Frazer C S, Snow C S, Tissot R G and Boespflug E P 2007 *Powder Diffr.* **22** 118